

# Material Transfer and Contact Optimization in MoS<sub>2</sub> Nanotube Devices

Robin T. K. Schock, Stefan Obloh, Jonathan Neuwald, Matthias Kronseder, Wolfgang Möckel, Matjaž Malok, Luka Pirker, Maja Remškar, and Andreas K. Hüttel\*

While the promise of clean and defect-free MoS<sub>2</sub> nanotubes as quantum electronic devices is obvious, ranging from strong spin-orbit interaction to intrinsic superconductivity, device fabrication still poses considerable challenges. Deterministic transfer of transition metal dichalcogenide nanomaterials and transparent contacts to the nanomaterials are nowadays highly active topics of research, both with fundamental research and applications in mind. Contamination from transport agents as well as surface adsorbates and surface charges play a critical role for device performance. Many techniques have been proposed to address these topics for transition metal dichalcogenides in general. Herein, their usage for the transfer-based fabrication of MoS<sub>2</sub> nanotube devices is analyzed. Further, different contact materials are compared in order to avoid the formation of a Schottky barrier.

## 1. Introduction

Since the first experimental isolation of graphene,<sup>[1]</sup> the field of 2D materials has grown immensely.<sup>[2–6]</sup> One prominent group of such materials is given by transition metal dichalcogenides (TMDCs),<sup>[2]</sup> consisting of a layer of transition metal atoms (e.g., tungsten, molybdenum) sandwiched between two layers of chalcogenides (e.g., sulfur, selenium, tellurium). MoS<sub>2</sub>, a member of this group,

is a typically n-doped semiconductor with a strong spin-orbit interaction. In its monolayer form, broken inversion symmetry causes spin split bands.<sup>[2]</sup> In addition, even in the monolayer limit it can be driven into intrinsic superconductivity via ionic doping;<sup>[7,8]</sup> for hole conduction, theory predicts it to be a topological superconductor.<sup>[9–11]</sup>

Many attempts have been made to define quantum dots (QDs) in planar TMDC materials.<sup>[12]</sup> However, the typically large effective electron mass in the conduction band requires minuscule device sizes at the limits of traditional lithography, and most observations so far are limited to classical, metallic Coulomb blockade<sup>[13–17]</sup> and QDs at defects.<sup>[18–20]</sup> Only very recently quantization effects have been observed

in lithographically defined systems.<sup>[21,22]</sup> TMDC-based nanotubes<sup>[23]</sup> could naturally provide strong confinement in an additional dimension as well as perfect electronic boundary conditions compared to lithographically defined nanoribbons.

The challenging fabrication of long and defect-free MoS<sub>2</sub> nanotubes,<sup>[24]</sup> higher radii compared to carbon nanotubes (CNTs),<sup>[25]</sup> and the fact that only multiwall nanotubes have been isolated up to now, have so far limited research. Additionally, the TMDCs where stable and defect-free nanotubes have been produced, are typically semiconductors. Metal contacts form Schottky barriers, resulting in large contact resistances.<sup>[26]</sup> Strong Fermi level pinning has been observed,<sup>[27,28]</sup> further complicating the situation. For planar TMDCs, recently remarkable advances in circumventing these barriers were made.<sup>[29–31]</sup> Regarding nanotubes, for a long time research was limited to optical and mechanical properties,<sup>[32,33]</sup> and work addressing superconductivity in WS<sub>2</sub>.<sup>[34]</sup> First attempts of low-temperature transport spectroscopy used metals with a suitable low-work function,<sup>[35,36]</sup> but these metals were shown to react with and destroy the crystal lattice of MoS<sub>2</sub>.<sup>[36–38]</sup> Only recently, using the semimetal bismuth led to a breakthrough.<sup>[39]</sup>

Here, we utilize state of the art transfer techniques adapted from 2D materials<sup>[40,41]</sup> and classical semiconductor fabrication to build electronic devices integrating MoS<sub>2</sub> nanotubes. We compare these techniques in terms of device yield and describe their effects on the device. Overall, surprisingly, the devices fabricated with the classical “Scotch tape” method alone perform better than any of the more sophisticated transfer techniques. Additionally, we investigate several contact materials, extending our previously published results.<sup>[39]</sup> Still bismuth remains, so far, the best candidate for contacting MoS<sub>2</sub> nanotubes.


R. T. K. Schock, S. Obloh, J. Neuwald, M. Kronseder, W. Möckel, A. K. Hüttel

Institute for Experimental and Applied Physics  
University of Regensburg  
93053 Regensburg, Germany  
E-mail: andreas.huettel@ur.de

M. Malok, L. Pirker, M. Remškar  
Solid State Physics Department  
Institute Jožef Stefan  
1000 Ljubljana, Slovenia

L. Pirker

J. Heyrovský Institute of Physical Chemistry, v.v.i.  
Czech Academy of Sciences  
18223 Prague, Czech Republic

 The ORCID identification number(s) for the author(s) of this article can be found under <https://doi.org/10.1002/pssb.202400366>.

© 2024 The Author(s). physica status solidi (b) basic solid state physics published by Wiley-VCH GmbH. This is an open access article under the terms of the Creative Commons Attribution License, which permits use, distribution and reproduction in any medium, provided the original work is properly cited.

DOI: 10.1002/pssb.202400366

## 2. MoS<sub>2</sub> Nanotube Growth

In this work, we use MoS<sub>2</sub> nanotubes grown by an iodine-assisted chemical transfer process.<sup>[24,42,43]</sup> This technique utilizes the migration of the gas phase of a metal compound along a temperature gradient from an area of vaporisation to an area of crystallisation. A halogen, in this case iodine, functions as transport agent.

The precursor, bulk crystalline MoS<sub>2</sub>, is given into a quartz glass ampoule together with iodine I<sub>2</sub>, see **Figure 1a,b**. The ampoule is subsequently evacuated and sealed by locally melting the quartz glass. It is then heated up in a tube oven under presence of a temperature gradient, with the precursor MoS<sub>2</sub> placed at the hotter end. Remaining oxygen O<sub>2</sub> emitted from the quartz glass ampoule walls also participates in the reaction. The precursor reacts according to  $\text{MoS}_2 + \text{I}_2 + \text{O}_2 \rightarrow \text{MoI}_2\text{O}_x + \text{S}_2$ , with the gaseous products then migrating along the temperature gradient to the cooler recrystallisation area, see **Figure 1a**.<sup>[42]</sup> There, the reverse process,  $\text{MoI}_2\text{O}_x + \text{S}_2 \rightarrow \text{MoS}_2 + \text{I}_2 + \text{O}_2$ , takes place. Subsequently the transport agents diffuse back to the hotter end, leading to a continuous process as long as the temperature gradient is maintained and feed material is present.

Over a growth period of  $\approx 500$  h, clean and long nanotubes with a very low defect density form on the growth side, accompanied by ribbon-like collapsed nanotubes, platelets, flakes, and more complex structures. After a slow cool-down, the quartz glass ampoule is broken apart in order to access the grown and deposited material. Example images of growth results can be found in **Figure 1c–e**.

## 3. Transfer and Assembly Techniques

Over the past decade, for research on 2D materials many different material transfer and assembly techniques have been developed, and this process is still ongoing. In the following, we

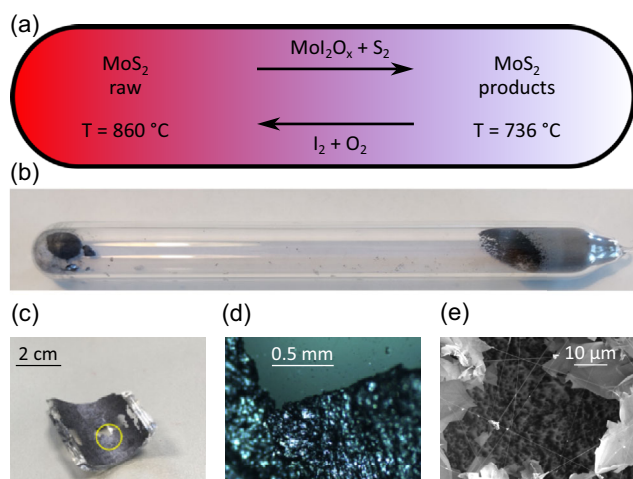


**Figure 1.** MoS<sub>2</sub> nanotube growth: a) schematic of the chemical transport growth reaction, b) photograph of a growth ampoule containing the source material and the reaction result, c,d) optical images of the resulting material on a piece of a broken ampoule, and e) scanning electron micrograph of the material displaying MoS<sub>2</sub> nanotubes and flakes.

discuss the usage of some of these methods for MoS<sub>2</sub> nanotube devices. In general, more complex transfer methods are developed to avoid contamination by the transfer agents and achieve cleaner results. As an example, the anthracene crystal-based method detailed in Section 3.5 has been used by Otsuka et al. with carbon nanotubes, leading to photoluminescence spectra fully comparable to as-grown macromolecules and thus indicating negligible contamination effects.<sup>[40]</sup>

### 3.1. The “Scotch Tape” Method

A very straightforward procedure to integrate MoS<sub>2</sub> nanotubes into electronic devices is the classical “Scotch tape”, “blue tape”, or “Nitto tape” method initially developed for graphene,<sup>[1]</sup> as illustrated in **Figure 2**. Nitto Denko ELP BT-150E-CM adhesive tape is pressed onto the raw MoS<sub>2</sub> material on a piece of the glass ampoule. Then the same piece of tape is pressed onto a silicon wafer with a thermally grown 500 nm thick oxide layer and predefined chromium-gold position markers. This randomly transfers nanotubes, flakes, and other MoS<sub>2</sub> nanostructures onto the chip surface at an adjustable surface density. While the process is fairly straightforward and applies to a comparatively large target area, also a small part of the adhesive coating is deposited, leading to sticky patches and some contamination.

In order to contact specific nanotubes, their position on the chip is then determined by optical microscopy. Surprisingly, even small diameter MoS<sub>2</sub> nanotubes can be detected this way; we attribute the clear visibility to their outstanding optical properties.<sup>[38,44]</sup> The optical images, including position markers, are used as a base for the design of contact geometries. The chip is then spin-coated with polymethyl metacrylate (PMMA) resist; after a standard electron beam lithography (EBL) process, the contact metallization is deposited onto the exposed parts of

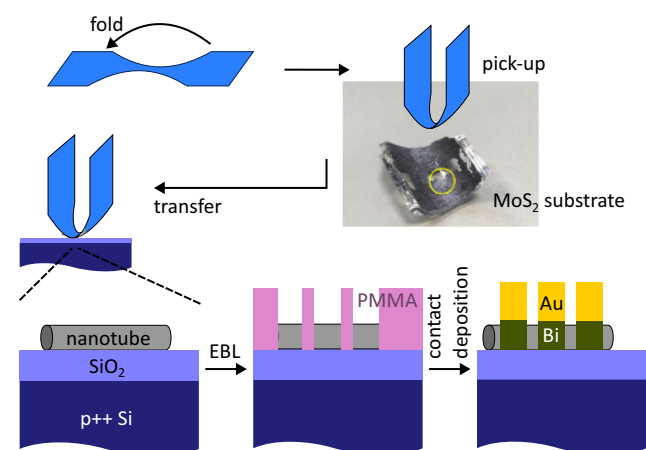


**Figure 2.** Schematic of the “Scotch tape” (or “Nitto tape”) method as applied here. First a piece of Nitto Denko ELP BT-150E-CM tape is cut into a strip narrowing in the middle. Then the strip is folded and softly pressed onto the MoS<sub>2</sub> nanotube growth substrate, a piece of the original quartz ampoule. This way nanotubes are picked up and can then be placed onto a receiving p-doped Si–SiO<sub>2</sub> substrate. Subsequently, using a standard EBL process, metal evaporation/sputtering, and lift off, contacts are defined on the nanotubes.

the nanotubes and lift-off in hot acetone is performed, see Figure 2 and the discussion of the different materials below.

### 3.2. Suspending Nanotubes between Contacts

This process can be altered in order to reduce the disorder caused by the amorphous SiO<sub>2</sub> surface and its surface charges; from carbon nanotubes it is well-known that suspending the nanostructures leads to significantly better spectroscopic results.<sup>[45,46]</sup> Prior to stamping the nanotubes onto the sample, a PMMA resist is deposited onto the surface. The stamp transfer works equally well for the blank SiO<sub>2</sub> surface and the hardened PMMA layer. After the transfer, a second PMMA layer is then spincoated onto the first resist, such that the nanotubes are ideally located at the interface between both layers. After electron beam lithography and development of the resist, the nanotubes are then suspended at the height of the interface between the two resist layers, held in place between remaining, nonexposed resist areas. Following the contact material deposition and resist removal, they are then suspended between the contacts themselves.

The bottom resist layer was spin-coated using a “1% to 4% PMMA 50k” solution, that is, a solution of 1% to 4% by weight of PMMA in anisol, where the average molecular weight of the PMMA polymer chains is 50 000 u. This resulted in a resist thickness range of 20–60 nm, comparable to or less than the nanotube diameters. Alternatively, for a higher likelihood of a finite gap between chip substrate and nanotube, a 9% PMMA 200k solution, that is, a solution of 9% by weight PMMA of average molecular weight 200 000 u in anisol, was used, leading to a resist layer thickness of about 200 nm. For the top layer in either case 9% PMMA 200k was applied. Different metallizations were tested, see also the discussion and the SEM images in Figure 8, Section 4.3 below, where the quality of the resulting contacts is discussed. A typical thin contact layer would consist of 40 nm bismuth and 50 nm gold, both thermally evaporated; later experiments tested thicker but similar metallization layers.

### 3.3. Polydimethylsiloxane Transfer

Polydimethylsiloxane (PDMS) is a silicon-based polymer widely used in 2D material science as a substrate and as a transfer agent.<sup>[41,47]</sup> This is due to its flexibility and viscoelastic properties, which make the transfer of 2D flakes (and nanotubes) between different substrates possible.

Here, PDMS was primarily used to transfer quasi-2D hexagonal boron nitride (hBN) and few layer graphene onto Si/SiO<sub>2</sub> substrates with predefined gold structures on them, as highly conductive back gate and crystalline gate isolator without dangling bonds. Literature on bilayer graphene has amply demonstrated that this sort of material stack reduces disorder from the amorphous surface of SiO<sub>2</sub> as well as provides a very homogeneous electric field.<sup>[48–52]</sup> While the transfer does not directly involve the MoS<sub>2</sub> nanotubes, we include it here for completeness.

Material transfer is achieved by at first pressing a ribbon of Nitto tape onto a bulk piece of the material in question, thereby retrieving a small amount of the 2D material, see Figure 3. Subsequently, the tape is folded, pressed together, and then ripped apart in order to break up the bulk stacks into smaller

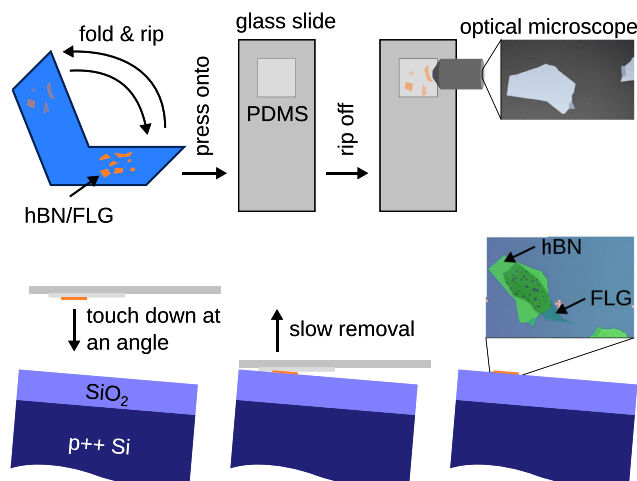


**Figure 3.** Schematics of the polydimethylsiloxane (PDMS) transfer method, mostly used for few layer graphene (FLG) and hexagonal boron nitride (hBN) flake transfer. First a piece of Nitto tape is cut into a strip and pressed upon the bulk substrate of the transfer material, for example, hBN. Then the strip is folded onto itself and ripped apart repeatedly in order to thin down the material. By pressing a piece of PDMS of  $\approx 1 \times 1$  cm onto the Nitto tape and ripping it off, some of the flakes are transferred onto the PDMS. After determining the position of a flake with an optical microscope, the flakes are transferred onto a SiO<sub>2</sub>/Si substrate.

stacks and potentially monolayers of the 2D materials. This process is repeated at least 10 times.

A piece of a flat PDMS film, commercially available as Gelpak Gelfilm, is attached to a glass slide and pressed onto the adhesive tape with the exfoliated 2D materials. Using a very fast peel-off, some of the flakes are transferred onto the PDMS film. The film is then inspected in an optical microscope. Finally, flakes of the desired size and thickness are carefully pressed onto a receiving SiO<sub>2</sub> substrate and then remain on the surface when peeling off the PDMS very slowly.

### 3.4. Polycarbonate Transfer

This method, for targeted transfer of a nanostructure from one substrate to a specific position on a different one, builds upon the two previous recipes. A PDMS drop is used as stamp substrate, with a polycarbonate (PC) film covering its surface to avoid direct contact between nanostructure and PDMS.

First, a thin layer of poly(bisphenol A carbonate) is fabricated through coating a glass slide with a chloroform-PC solution of 4%. The coating is subsequently air-dried. The resulting PC layer is slowly peeled off the glass slide using an adhesive tape with a cutout area in the middle. The PC-tape stack is then placed onto a premade PDMS droplet on another glass slide, where it is secured such that the exposed PC layer is stretched over the droplet. The resulting PC-film-coated droplet is then carefully pressed onto a substrate with an isolated, previously exfoliated nanotube or flake, heated to 130 °C, and slowly peeled off, effectively picking up the material.

The resulting stack, consisting of the flake or nanotube, the PC layer, and the PDMS droplet on a glass carrier, is subsequently

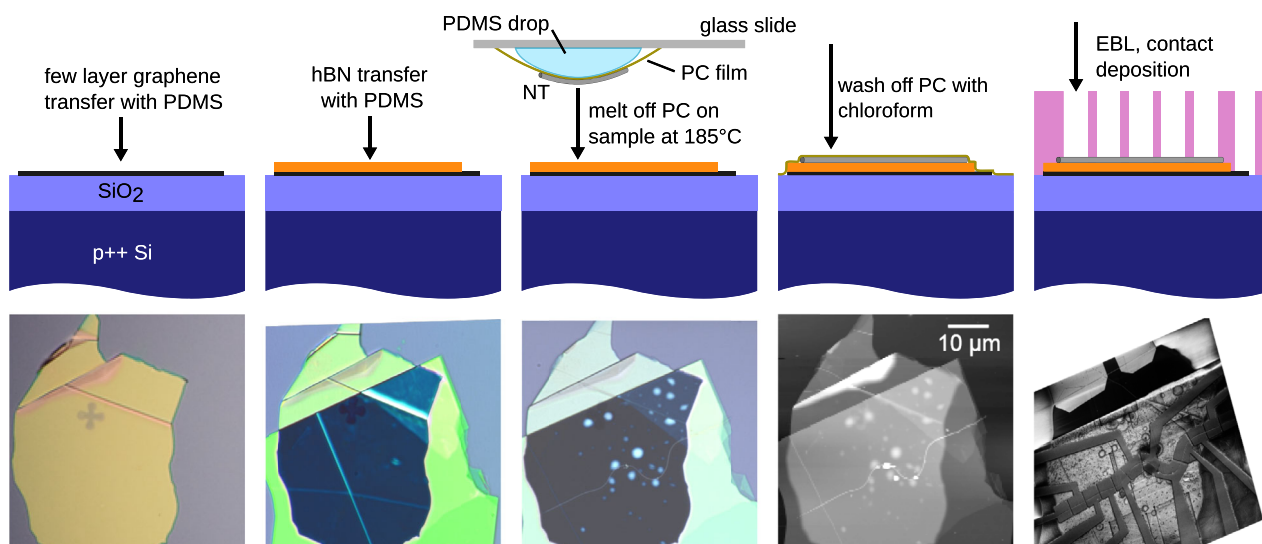


**Figure 4.** Schematics of the polycarbonate (PC)-assisted transfer method. In the first step, few layer graphene (FLG) and hBN are transferred with the “PDMS method” (see Figure 3) and stacked upon each other. Then a previously prepared strip of a thin PC film is placed and fixed upon a PDMS droplet on a glass slide. In an xyz-stage, a nanotube is picked up from a silicon wafer (prepared with the “Scotch tape method”, see Figure 2). The nanotube is placed upon the FLG-hBN heterostack, and the PC is molten at 185 °C. Afterwards, the PC is washed off with chloroform and the nanotube is contacted through standard EBL processing.

pressed onto a receiving substrate and heated to 185 °C, causing the PC to melt, see **Figure 4**. As the PDMS is lifted, the liquefied PC with the attached nanomaterial structure remains on the sample. Finally, the PC layer is gently washed off in hot chloroform for 15 min, leaving the nanotube or flake on the substrate.

Compared to direct transfer with only PDMS, this procedure has two main advantages. Due to the melting of the PC film, it is possible to transfer materials which adhere stronger to PDMS than to the receiving substrate. Further, as there is no direct contact between the flakes/nanotubes and the PDMS, any contamination from PDMS is washed off together with the PC in the chloroform rinsing step.

### 3.5. Anthracene-Assisted Transfer

In case even the PC film transfer introduces too much contamination, a recently developed replacement procedure utilizes anthracene crystals as alternative intermediate transfer agent between PDMS and the flakes or nanotubes.<sup>[40]</sup> To implement this method, also illustrated in **Figure 5**, we first grow anthracene crystals on glass slides suspended 1 mm above granular anthracene heated to 80 °C in an ambient atmosphere. In order to grow large and thin single crystals with a size of about 1 mm<sup>2</sup>, following Otsuka et al.<sup>[40]</sup> a commercial permanent marker was used to draw black lines on the glass slide, see Figure 5. In the marked, dark regions, the growth of crystals is suppressed; crystals growing nearby can extend above this region and then reach larger sizes. The initial publication used a permanent marker of type KOKUYO PM-41B; we found the type STAEDLER permanent Lumocolor S, Nr. 313-9 to be a suitable replacement. After a growth period of about 12 h, large and homogeneous anthracene single crystals form on the slides.

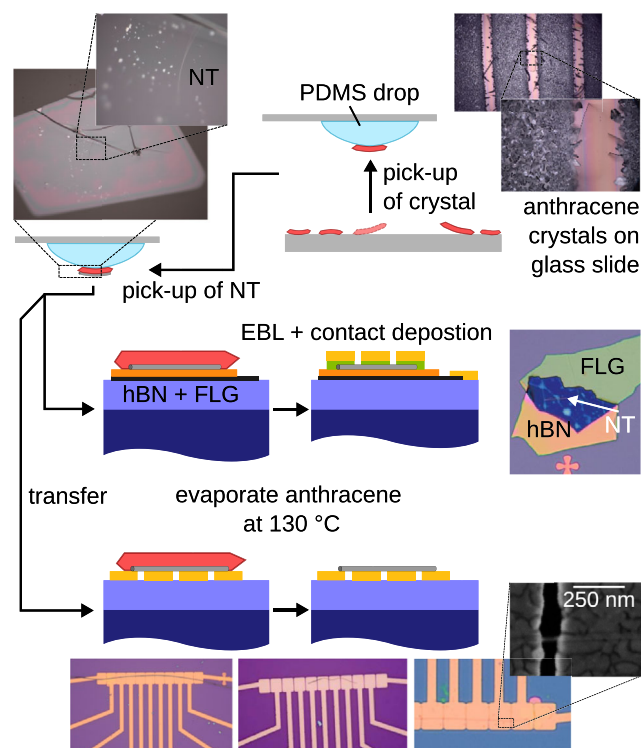


**Figure 5.** Anthracene crystal-assisted transfer of a nanotube. First, anthracene crystals are grown on a glass slide. Then, a large anthracene crystal is picked up with a PDMS drop. With this, a nanotube, exfoliated with the scotch tape method, or a 2D flake (hBN or FLG) can be picked up. These can then be either placed onto a heterostack (middle part) or transferred onto predefined contacts (lower part). The anthracene crystal with the material is pressed onto the chip and remains there if peeled off slowly. After that, the anthracene is sublimated by heating the device above 130 °C.

With an optical microscope in a transfer setup, suitable crystals were chosen and picked up with a PDMS droplet, see Figure 5. Similar to the PC-based method, the anthracene crystal was pressed upon a flake or nanotube and the substrate was subsequently heated to a temperature of above 80 °C in order to increase the adhesion of the anthracene to the object to be transferred. Then, the nanotube, anthracene, and PDMS stack was rapidly peeled off (in under a second) to ensure that the anthracene adheres more strongly to the PDMS than to the SiO<sub>2</sub> chip surface. In order to deposit the nanomaterial at the top of the stack, it was pressed upon the desired location of the receiving chip, heated to a temperature above 90 °C, and very slowly peeled off over a duration of about 1 min, which left the anthracene with the transferred stack on the surface of the chip. The anthracene crystal was then sublimated by heating to a temperature above 130 °C; it typically leaves no visible contamination residues.

As shown in Figure 5, this method allows for two different approaches to device fabrication. Either a heterostack can be assembled with subsequent deposition of top contacts, or the nanotube can be placed upon predefined contacts with trenches between them. As the anthracene evaporates in an ambient atmosphere, without the need of any wet chemical processing, there is no danger of ripping off thin layers or nanotubes due to surface tension.<sup>[40]</sup> Using predefined contacts is obviously limited to contact materials which do not form an insulating oxide barrier in ambient atmosphere, unless additional encapsulation steps are performed.

## 4. Contact Engineering

For all the deposition of nanotubes and/or layer assembly of devices, achieving good electrical contacts to the nanomaterial is of central importance. In particular, here we talk about transparent and nondestructive contacts:<sup>[39]</sup> transparent meaning having a low resistance and Ohmic behaviour, and nondestructive meaning that the contact fabrication does not significantly damage the molecular and thereby electronic structure of the nanomaterial.

For planar, quasi-2D MoS<sub>2</sub>, a large amount research has been invested into this topic worldwide, with the primary objective of Ohmic contacts for MoS<sub>2</sub>-based field effect transistors. As with many other TMDC materials, strong Schottky barriers typically form at the semiconductor–metal interface.<sup>[26,53]</sup> The precise mechanisms involved in their formation have long been under discussion. While the mismatch of the metal work function certainly contributes, see the discussion below, additionally strong Fermi level pinning takes place at the interface.<sup>[27,28,54,55]</sup>

In the case of MoS<sub>2</sub> nanotubes, the reduced geometry poses additional difficulties. An edge contact to a MoS<sub>2</sub> flake is effectively a one-dimensional interface; the same edge contact to a nanotube however zero-dimensional. Further, while graphene has been shown to make good contacts to planar MoS<sub>2</sub> and other TMDC,<sup>[56]</sup> so far no such success has been achieved by depositing a “flat” graphene or graphite layer onto a “round” nanotube or vice versa—an observation which can likely be attributed to the shape mismatch.

### 4.1. Impact of the Contact Material

Several different approaches to avoid the formation of a Schottky barrier at metallic contacts to MoS<sub>2</sub> have been proposed so far. Primarily these revolve around the selection of the contact material. In classical semiconductor technology, a Schottky barrier is minimized by adapting the metal work function to the semiconductor. For MoS<sub>2</sub> with an electron affinity of  $\chi_{\text{MoS}_2} = 4.0$  eV, this means selecting a *low-work function metal* such as titanium or scandium.<sup>[31,36,37]</sup> In the following, we name this a *type-I contact*. As demonstrated previously,<sup>[36]</sup> scandium can be used to contact MoS<sub>2</sub> nanotubes, however, serial charge traps make Coulomb blockade spectroscopy difficult. In hindsight, the origin of these charge traps is obvious—the chemically reactive metal destroys the MoS<sub>2</sub> layer structure already during deposition.<sup>[37]</sup>

Inserting a thin insulating layer (e.g., an insulating hBN monolayer) as a *transparent tunneling barrier*, which at the same time prevents Schottky barrier formation, has been attempted with some success on 2D materials.<sup>[57–60]</sup> Accordingly this was also tested for MoS<sub>2</sub> nanotubes, see the discussion below, and named *type-II contact*. Local doping in the contact areas is another technique transferred from existing semiconductor technology.<sup>[61,62]</sup> For nanotubes, the small relevant surface area makes this difficult to implement; in addition, surface dopants immediately lead to potential irregularities that would pose problems in low-temperature measurements. Since copper doping has shown promise in other works,<sup>[63]</sup> we also have tested bulk copper contacts.

Recently, it was discovered, that the use of *semimetals* was a promising way to avoid the formation of strong Schottky barriers at a MoS<sub>2</sub> interface.<sup>[29]</sup> In the interface region of a semiconductor and a metal, hybridization of the electronic bands of the semiconductor and the metal leads to so-called metal-induced-gap-states (MIGS) and via them to Fermi level pinning.<sup>[64]</sup> The density of states (DOS) of a semimetal however approaches zero at the Fermi level, leading to a corresponding reduction in MIGS. This in turn reduces stability of the Schottky barrier and makes Ohmic contacts possible.<sup>[29,30,39]</sup> Graphene has already been used to contact planar MoS<sub>2</sub>,<sup>[56]</sup> attempts with MoS<sub>2</sub> nanotubes have failed so far however, most likely due to the mismatch in shape/geometry. This leads us to the elements bismuth<sup>[29,39]</sup> and antimony,<sup>[30,65]</sup> already highly successful for planar materials, as contact layers. This approach is in the following named *type-III contact*.

The devices prepared in this work were measured under ambient conditions. The two-point resistance was determined by applying a constant bias voltage of 10 mV and measuring the resulting current. The resulting values for different contact materials are shown as scatter plots in **Figure 6**, with the median of each material given as horizontal line and written out above the corresponding column. We do not differentiate between deposition methods here, though the large majority of devices was fabricated using the simplest “Scotch tape” transfer, either on the chip surface (see Section 3.1) or on a predeposited resist layer (see Section 3.2). Bismuth-based semimetal contacts (i.e., *type-III*) clearly outperformed all other tested materials, with a median two-point resistance value of  $R_{\text{Bi}} = 2 \text{ M}\Omega$ .<sup>[29,39]</sup> This confirms corresponding work on planar MoS<sub>2</sub> as well as our own previous publication.<sup>[39]</sup>

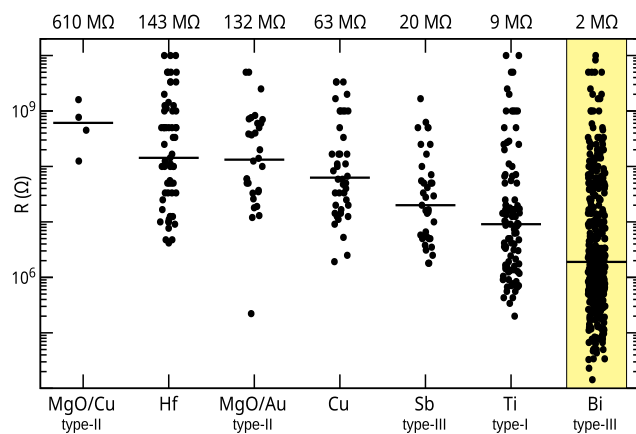


**Figure 6.** Two terminal resistances of MoS<sub>2</sub> nanotubes and nanoribbons contacted with different contact materials. Each point in the graph corresponds to the room-temperature resistance measured between two contacts on a nanotube or nanoribbon. Additionally, the median resistance for each material is marked with a black line. Clearly, bismuth leads to the smallest median resistance, an order of magnitude smaller than the second best tested material titanium. Part of the data has already been shown previously.<sup>[39]</sup>

The material with the second best median two-point resistance was titanium. It is a metal with a well-suited work function for n-type conduction band contacts to MoS<sub>2</sub> (i.e., *type-I*), however has also shown to be highly reactive.<sup>[37]</sup> Similar results and disadvantages have been seen for scandium.<sup>[36]</sup> As such, even though the room-temperature results are promising, charge traps and potential irregularities at the contacts will likely make low-temperature transport spectroscopy challenging.

Aside bismuth, also the semimetal antimony has been used to successfully make contacts to planar TMDC materials.<sup>[30]</sup> However, for our nanotubes the results using antimony were already significantly worse, with a median value  $R_{Sb} = 20 \text{ M}\Omega$ . Note that Li et al. only achieved their best contact resistances with antimony grown in the (01 $\bar{1}2$ ) direction, depositing the contacts under elevated temperatures of about 100 °C.<sup>[30]</sup> In contrast, here, the antimony was deposited at room temperature, and no clear statement on its crystal orientation was possible. In addition, compared to planar MoS<sub>2</sub>, where a topmost layer can be matched by the crystal structure of the contact material, nanotubes expose a curved surface to the semimetal. This likely prevents, even locally, the formation of a single crystalline layer with a matching structure.

Further material combinations tested include gold and copper—as well-conducting metals with a large electronic density of states—on top of a thin MgO tunnel barrier, that is, *type-II* contacts. As visible in Figure 6, in both cases the resulting two-point resistances are comparatively high. Even given the scatter and the still relatively small number of data points, further investigations seem not worthwhile, with median two-point resistance values of 610 and 132 MΩ.

#### 4.2. Impact of the Transfer Technique

In Figure 7, we compare the observed two terminal resistances of devices prepared with different transfer techniques. In all cases,

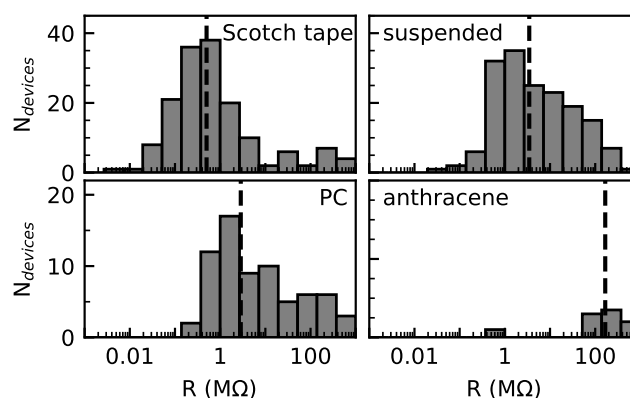


**Figure 7.** Two terminal resistance distributions of bismuth-contacted nanotube devices, for four different material transfer methods—“Scotch tape” deposition (Section 3.1), suspended nanomaterial (Section 3.2), polycarbonate-assisted deposition (Section 3.4), and anthracene-assisted deposition (Section 3.5).

bismuth has been used as the contact layer. As clearly visible from the figure, so far, the simplest “Scotch tape” transfer technique shows the best results, with a much larger number of devices exhibiting two terminal resistances below 1 MΩ. Both suspending the nanomaterial (see Section 3.2) and PC transfer (see Section 3.4) seem to have a negative impact on the fraction of devices produced with a two-point resistance below 1 MΩ. Additionally, much more devices with resistances above 10 MΩ can be observed, indicating a reduced quality of the contacts.

The validity of the evaluation is limited insofar as the fabrication using more complex methods mostly took place at a later time and used later nanomaterial growth batches; a hypothetical change in clean room chemicals quality, raw material properties (which we do not have any further indications of), etc., would materialize similarly in the plots.

As for the anthracene method, only a very small number of devices was tested so far. All the data in Figure 7 for anthracene devices stems from contacts to a total number of four nanotubes prepared in two different ways; it can only tentatively indicate that this approach also reduces contact quality. The chips with device resistances above 100 MΩ were prepared with contacts predefined by EBL procedure and a channel length of about 100 nm. In the two devices on one nanotube with resistances below 1 MΩ, the nanotube was transferred onto gold contacts presliced with the beam of a focused ion beam (FIB) system. The channel length in these devices was at about 50 nm much smaller than that of other device types, which may contribute to slightly lower device resistance. Further, it is conceivable that the Ga<sup>+</sup> ions deposited by the FIB beam in the vicinity of the trenches dope the surface of the nanotubes and therefore lower the Schottky barrier. With only one nanotube tested so far, these ideas are however only speculative and require further investigation.

#### 4.3. SEM Failure Analysis

The large scatter of the resistance data points in Figure 6 and 7 even in the case of nominally identical device preparation

indicates that the fabrication process still has fundamental limitations. To identify problems, several devices were imaged in detail in a scanning electron microscope; example results can be seen in **Figure 8**.

A possible cause of the reduced contact quality is the occurrence of gaps or cracks between the contact material deposited on top of the nanotube and the contact material deposited next to them, see, for example, the black arrow in **Figure 8a**. While not occurring for carbon nanotubes due to their much smaller radius, this is a well-known (and sometimes intended) phenomenon when evaporating materials onto elevated structures such as semiconductor nanowires. Due to the directional material deposition via thermal evaporation, a contact material “cap” forms on the top of the nanotube. As the cap grows, it begins to shadow a larger area below and next to the nanotube, reducing deposition in that region. A precise adjustment of the contact material thickness to the nanomaterial dimensions, in order to counteract this, is in our case challenging since typically nanotubes and ribbons of varying size are deposited on the same chip.

Initial resistance testing of devices suggested an optimum of the electronic behaviour around the contact layer thickness used to fabricate the device of **Figure 8a**.<sup>[39]</sup> However, as explained earlier, if the contact material films are not thick enough, the cap of contact material on top of the nanostructure and the surrounding contact material may not consistently reach each other. As found out subsequently, this is possible in the region indicated with an arrow in the SEM image of **Figure 8a**, indicating the need for a more robust contact metallization.

In addition, the SEM images of devices suggest grain-based growth of the contact films, especially for bismuth, with

corresponding fluctuation of the layer thicknesses and potential gap sizes. Even in presence of a gap, contact could still occur occasionally. This is not limited to the suspended nanotube case, but is very likely to be more dominant there, which could further explain the wide scatter of contact resistances for all materials and the slightly worse results for devices intended to feature suspended nanotubes.

In order to prevent the gap formation, the contacts deposited in **Figure 8b** were significantly thicker; in addition, thermal evaporation of the contact materials was done at two separate angles of device orientation to improve coverage. Preliminary results indicate that this could at least partially improve the contact quality; one of two devices fabricated so far had several contacts with resistances below 1 M $\Omega$ . The second one, with the nanoribbon depicted in **Figure 8b**, performed much worse, clearly since almost all nanoribbons and -tubes were ripped out of the embedding material. The reason for this is unclear so far.

## 5. Discussion of the Resistance Scatter

Of all tested contact materials, the bismuth–gold combination so far remains the most promising one—in combination with the least sophisticated fabrication method. Nevertheless, the observed two-point resistances scatter widely. What is the cause?

A *wide distribution of nanomaterial properties* cannot be fully excluded. The MoS<sub>2</sub> growth process delivers flakes, nanotubes, nanoribbons as well as breathing and twisted variants.<sup>[24,66]</sup> During the transfer process, long, straight, and thin structures are preferably selected in the optical microscope. Distinguishing nanotubes from nanoribbons and determining the precise dimensions would however require time-consuming SEM or atomic force microscopy (AFM) imaging, which may also lead to additional contamination or damage.

*Contamination during lithography*, as, for example, organic resist residues or reactions with photoresists or -developers, is another relevant topic. Moving the fabrication away from optical lithography to electron beam lithography with its organic chemistry only has so far not led to clear improvements. Imperfect dissolution of resist layers during development is possible. While the resist remainders can in principle be removed with a brief oxygen plasma based descum process, the plasma treatment will strongly attack the sulphur surface and have an impact on its own.<sup>[67–69]</sup>

*PDMS or PC contamination during stamping* can reduce the device quality. It is already known that PDMS contaminates the surface of 2D materials after the stamping process.<sup>[40,70,71]</sup> As both FLG and hBN were transferred using PDMS this can introduce disorder in the heterostack, degrading the quality of the backgate. Additionally, contamination on the hBN surface is in direct contact with the nanotubes and could influence its electronic properties. Finally, during the PC transfer of the nanotube, residues of PDMS may spread onto the contact surface of the nanotube. Together with contamination from the PC itself,<sup>[70]</sup> these would be directly at the nanotube-semimetal interface.

*Insufficient metallization or metallization gaps* at the contacts can, as discussed already above, particularly affect large-diameter nanomaterials and suspended structures. One may also speculate that too thick bismuth regions become nonconductive at

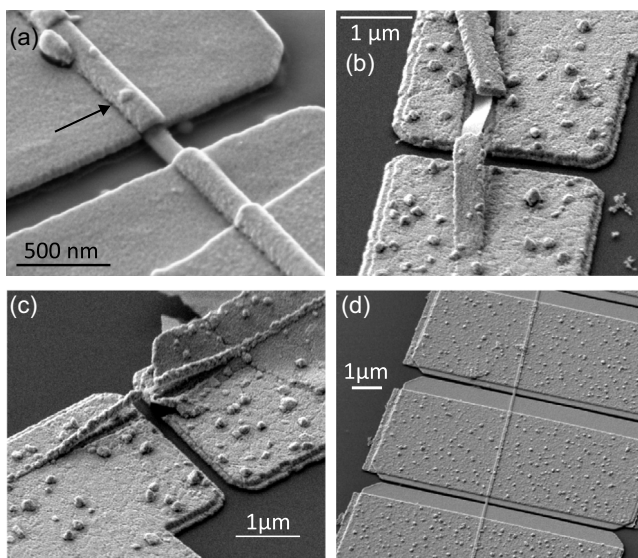


**Figure 8.** SEM images of devices after fabrication and probe station characterization. a) Nanotube contacted with a bismuth layer of 40 nm and a gold layer of 50 nm; b) nanoribbon and c) nanotube on the same sample contacted with a bismuth layer of 50 nm and a gold layer of 100 nm both evaporated under two different angles, resulting in a step-like perimeter; d) nanotube transferred with anthracene onto 100 nm gold contacts with  $\approx 100$  nm gaps and subsequently contacted with 25 nm bismuth and 30 nm gold, both evaporated at two different angles.

low temperature, leading to additional resistive barriers. Metal deposition under varying angles and thicker gold cap layers should be used to mitigate these effects.

*Tear-off of the nanomaterial* has been observed, for example, in Figure 8b,c, as also discussed earlier; while the nanotube or nanoribbon remains whole, it entirely or in part lifts out of the contact electrodes, taking part of the material with it. Again thicker metallization, here combined with a more careful lift-off procedure, may be required. Surface tension during drying would pull a possibly suspended nanomaterial toward the substrate; we expect this to lead to different types of damage. Nevertheless, also the use of a critical point dryer may be considered for future devices.

## 6. Conclusions and Outlook

MoS<sub>2</sub> nanotubes and nanoribbons have significant potential for quantum electronic devices. Here, we compare different contact materials and material transfer techniques and their effect on the contacts to these MoS<sub>2</sub> nanomaterials.

Regarding the contact materials, we can so far conclude that the best choice for MoS<sub>2</sub> nanotubes and nanoribbons is bismuth,<sup>[29,39]</sup> a semimetal leading to the minimization of metal-induced gap states and Fermi level pinning. While, for planar MoS<sub>2</sub>, antimony, also a semimetal, has led to record conductivities,<sup>[30,65]</sup> this could not be confirmed for nanotubes. The comparison of different transfer techniques indicates that the classical “Scotch tape” method<sup>[1]</sup> in its simplicity still gives the most reliable results. We tentatively conclude that more complex fabrication procedures still pose more danger of surface contamination. A large scatter of measured resistance values remains, which can be due to several different causes. Insufficient coverage of the nonplanar nanomaterial and the formation of minuscule “nano-gaps” between the contact material covering the nanotubes and the contact material surrounding them, even at the apparent optimal layer thickness, seems to play an important role, with surface contaminations secondary in effect.

In order to reduce the impact of the nanogaps, multiple-angle evaporation as well as an overall thicker layer of contact material was used. First data indicate an improved likelihood of good contacts. Evaporation onto a heated device substrate as well as annealing are further approaches to be followed in the future. Regarding the reduction of potential surface contamination, O<sub>2</sub> and Ar plasma treatments shall be tested as next steps,<sup>[67–69]</sup> as well as H<sub>2</sub>S exposure of the devices at elevated temperature.<sup>[72]</sup> Even though clearly not all approaches apply to nanotubes and nanowires, the highly active worldwide research on planar MoS<sub>2</sub> field effect transistors provides a multitude of avenues to follow.

## Acknowledgements

The authors gratefully acknowledge funding by the DFG via grants Hu 1808/4-1 (project id 438638106) and Hu 1808/6-1 (project id 438640730) and by the Slovenian Research Agency via grant P1-0099. They would like to thank Lain-Jong Li for insightful discussions and Ch. Strunk and D. Weiss for the use of experimental facilities. The measurement data was recorded using Lab::Measurement.<sup>[73]</sup>

Open Access funding enabled and organized by Projekt DEAL.

## Conflict of Interest

The authors declare no conflict of interest.

## Data Availability Statement

The data that support the findings of this study are available from the corresponding author upon reasonable request.

## Keywords

contact, MoS<sub>2</sub>, nanotubes, optimization, transition metal dichalcogenides, transfer

Received: July 19, 2024

Revised: October 1, 2024

Published online:

- [1] K. S. Novoselov, A. K. Geim, S. V. Morozov, D. Jiang, Y. Zhang, S. V. Dubonos, I. V. Grigorieva, A. A. Firsov, *Science* **2004**, *306*, 666.
- [2] O. V. Yazyev, A. Kis, *Mater. Today* **2015**, *18*, 20.
- [3] K. S. Novoselov, A. Mishchenko, A. Carvalho, A. H. Castro Neto, *Science* **2016**, *353*, aac9439.
- [4] C. Tan, X. Cao, X. J. Wu, Q. He, J. Yang, X. Zhang, J. Chen, W. Zhao, S. Han, G. H. Nam, M. Sindoro, H. Zhang, *Chem. Rev.* **2017**, *117*, 6225.
- [5] S. Kang, D. Lee, J. Kim, A. Capasso, H. S. Kang, J. W. Park, C. H. Lee, G. H. Lee, *2D Mater.* **2020**, *7*, 022003.
- [6] S. Joseph, J. Mohan, S. Lakshmy, S. Thomas, B. Chakraborty, S. Thomas, N. Kalarikkal, *Mater. Chem. Phys.* **2023**, *297*, 127332.
- [7] J. M. Lu, O. Zheliuk, I. Leermakers, N. F. Q. Yuan, U. Zeitler, K. T. Law, J. T. Ye, *Science* **2015**, *350*, 1353.
- [8] D. Costanzo, S. Jo, H. Berger, A. F. Morpurgo, *Nat. Nanotechnol.* **2016**, *11*, 339.
- [9] Y. T. Hsu, A. Vaezi, M. H. Fischer, E. A. Kim, *Nat. Commun.* **2017**, *8*, 14985.
- [10] R. Oiwa, Y. Yanagi, H. Kusunose, *Phys. Rev. B* **2018**, *98*, 064509.
- [11] J. Wang, X. Zhang, R. Ma, G. Yang, E. V. Castro, T. Ma, *Phys. Rev. B* **2022**, *106*, 134513.
- [12] F. M. Jing, Z. Z. Zhang, G. Q. Qin, G. Luo, G. Cao, H. O. Li, X. X. Song, G. P. Guo, *Adv. Quantum Technol.* **2022**, *5*, 2100162.
- [13] Y. Li, N. Mason, From Coulomb Blockade to Resonant Transmission in a MoS<sub>2</sub> Nanoribbon, arXiv:1312.3939, **2013**.
- [14] C. S. Lau, J. Y. Chee, L. Cao, Z. E. Ooi, S. W. Tong, M. Bosman, F. Bussolotti, T. Deng, G. Wu, S. W. Yang, T. Wang, S. L. Teo, C. P. Y. Wong, J. W. Chai, L. Chen, Z. M. Zhang, K. W. Ang, Y. S. Ang, K. E. J. Goh, *Adv. Mater.* **2022**, *34*, 2103907.
- [15] X. X. Song, D. Liu, V. Mosallanejad, J. You, T. Y. Han, D. T. Chen, H. O. Li, G. Cao, M. Xiao, G. C. Guo, G. P. Guo, *Nanoscale* **2015**, *7*, 16867.
- [16] X. X. Song, Z. Z. Zhang, J. You, D. Liu, H. O. Li, G. Cao, M. Xiao, G. P. Guo, *Sci. Rep.* **2015**, *5*, 16113.
- [17] K. Lee, G. Kulkarni, Z. Zhong, *Nanoscale* **2016**, *8*, 7755.
- [18] N. Papadopoulos, P. Gehring, K. Watanabe, T. Taniguchi, H. S. J. van der Zant, G. A. Steele, *Phys. Rev. B* **2020**, *101*, 165303.
- [19] T. R. Devidas, I. Keren, H. Steinberg, *Nano Lett.* **2021**, *21*, 6931.
- [20] R. Krishnan, S. Biswas, Y. L. Hsueh, H. Ma, R. Rahman, B. Weber, *Nano Lett.* **2023**, *23*, 6171.
- [21] S. Davari, J. Stacy, A. Mercado, J. Tull, R. Basnet, K. Pandey, K. Watanabe, T. Taniguchi, J. Hu, H. Churchill, *Phys. Rev. Appl.* **2020**, *13*, 054058.

- [22] P. Kumar, H. Kim, S. Tripathy, K. Watanabe, T. Taniguchi, K. S. Novoselov, D. Kotekar-Patil, *Nanoscale* **2023**, *15*, 18203.
- [23] R. Tenne, L. Margulis, M. Genut, G. Hodes, *Nature* **1992**, *360*, 444.
- [24] M. Remskar, Z. Skraba, F. Cléton, R. Sanjinés, F. Lévy, *Appl. Phys. Lett.* **1996**, *69*, 351.
- [25] G. Seifert, T. Köhler, R. Tenne, *J. Phys. Chem. B* **2002**, *106*, 2497.
- [26] W. Schottky, *Z. Phys.* **1939**, *113*, 367.
- [27] C. Gong, L. Colombo, R. M. Wallace, K. Cho, *Nano Lett.* **2014**, *14*, 1714.
- [28] K. Sotthewes, R. van Bremen, E. Dollekamp, T. Boulogne, K. Nowakowski, D. Kas, H. J. W. Zandvliet, P. Bampoulis, *J. Phys. Chem. C* **2019**, *123*, 5411.
- [29] P. C. Shen, C. Su, Y. Lin, A. S. Chou, C. C. Cheng, J. H. Park, M. H. Chiu, A. Y. Lu, H. L. Tang, M. M. Tavakoli, G. Pitner, X. Ji, Z. Cai, N. Mao, J. Wang, V. Tung, J. Li, J. Bokor, A. Zettl, C. I. Wu, T. Palacios, L. J. Li, J. Kong, *Nature* **2021**, *593*, 211.
- [30] W. Li, X. Gong, Z. Yu, L. Ma, W. Sun, S. Gao, Ç. Koroglu, W. Wang, L. Liu, T. Li, H. Ning, D. Fan, Y. Xu, X. Tu, T. Xu, L. Sun, W. Wang, J. Lu, Z. Ni, J. Li, X. Duan, P. Wang, Y. Nie, H. Qiu, Y. Shi, E. Pop, J. Wang, X. Wang, *Nature* **2023**, *613*, 274.
- [31] S. Das, H. Y. Chen, A. V. Penumatcha, J. Appenzeller, *Nano Lett.* **2013**, *13*, 100.
- [32] M. Serra, R. Arenal, R. Tenne, *Nanoscale* **2019**, *11*, 8073.
- [33] J. L. Musfeldt, Y. Iwasa, R. Tenne, *Phys. Today* **2020**, *73*, 42.
- [34] F. Qin, T. Ideue, W. Shi, X. X. Zhang, M. Yoshida, A. Zak, R. Tenne, T. Kikitsu, D. Inoue, D. Hashizume, Y. Iwasa, *Nano Lett.* **2018**, *18*, 6789.
- [35] S. Fathipour, M. Remskar, A. Varlec, A. Ajoy, R. Yan, S. Vishwanath, S. Rouvimov, W. S. Hwang, H. G. Xing, D. Jena, A. Seabaugh, *Appl. Phys. Lett.* **2015**, *106*, 022114.
- [36] S. Reinhardt, L. Pirker, C. Bäuml, M. Remškar, A. K. Hüttel, *Phys. Status Solidi – Rap. Res. Lett.* **2019**, *13*, 1900251.
- [37] R. J. Wu, S. Udyavara, R. Ma, Y. Wang, M. Chhowalla, T. Birol, S. J. Koester, M. Neurock, K. A. Mkhoyan, *Phys. Rev. Mater.* **2019**, *3*, 111001.
- [38] M. Remskar, A. K. Hüttel, T. V. Shubina, A. Seabaugh, S. Fathipour, R. Lawrowski, R. Schreiner, *Isr. J. Chem.* **2022**, *62*, e202100100.
- [39] R. T. K. Schock, J. Neuwald, W. Möckel, M. Kronseder, L. Pirker, M. Remškar, A. K. Hüttel, *Adv. Mater.* **2023**, *35*, 2209333.
- [40] K. Otsuka, N. Fang, D. Yamashita, T. Taniguchi, K. Watanabe, Y. K. Kato, *Nat. Commun.* **2021**, *12*, 3138.
- [41] A. Castellanos-Gomez, M. Buscema, R. Molenaar, V. Singh, L. Janssen, H. S. J. van der Zant, G. A. Steele, *2D Mater.* **2014**, *1*, 011002.
- [42] R. Nitsche, *J. Phys. Chem. Solids* **1960**, *17*, 163.
- [43] M. Remškar, Z. Škraba, M. Regula, C. Ballif, R. Sanjinés, F. Lévy, *Adv. Mater.* **1998**, *10*, 246.
- [44] D. R. Kazanov, A. V. Poshakinskiy, V. Y. Davydov, A. N. Smirnov, I. A. Elisseyev, D. A. Kirilenko, M. Remškar, S. Fathipour, A. Mintairov, A. Seabaugh, B. Gil, T. V. Shubina, *Appl. Phys. Lett.* **2018**, *113*, 101106.
- [45] P. Jarillo-Herrero, S. Sapmaz, C. Dekker, L. P. Kouwenhoven, H. S. J. van der Zant, *Nature* **2004**, *429*, 389.
- [46] J. Cao, Q. Wang, H. Dai, *Nat. Mater.* **2005**, *4*, 745.
- [47] W. Dong, Z. Dai, L. Liu, Z. Zhang, *Adv. Mater.* **2024**, *36*, 2303014.
- [48] S. Engels, A. Epping, C. Volk, S. Korte, B. Voigtländer, K. Watanabe, T. Taniguchi, S. Trellenkamp, C. Stampfer, *Appl. Phys. Lett.* **2013**, *103*, 073113.
- [49] J. I. A. Li, C. Tan, S. Chen, Y. Zeng, T. Taniguchi, K. Watanabe, J. Hone, C. R. Dean, *Science* **2017**, *358*, 648.
- [50] L. Banszerus, B. Frohn, A. Epping, D. Neumaier, K. Watanabe, T. Taniguchi, C. Stampfer, *Nano Lett.* **2018**, *18*, 4785.
- [51] M. Eich, R. Pisoni, H. Overweg, A. Kurzmann, Y. Lee, P. Rickhaus, T. Ihn, K. Ensslin, F. Herman, M. Sigrist, K. Watanabe, T. Taniguchi, *Phys. Rev. X* **2018**, *8*, 031023.
- [52] H. Overweg, H. Eggimann, X. Chen, S. Slizovskiy, M. Eich, R. Pisoni, Y. Lee, P. Rickhaus, K. Watanabe, T. Taniguchi, V. Fal'ko, T. Ihn, K. Ensslin, *Nano Lett.* **2018**, *18*, 553.
- [53] J. R. Lince, D. J. Carré, P. D. Fleischauer, *Phys. Rev. B* **1987**, *36*, 1647.
- [54] W. Mönch, *Appl. Phys. Lett.* **1998**, *72*, 1899.
- [55] C. Kim, I. Moon, D. Lee, M. S. Choi, F. Ahmed, S. Nam, Y. Cho, H. J. Shin, S. Park, W. J. Yoo, *ACS Nano* **2017**, *11*, 1588.
- [56] A. Chanana, S. Mahapatra, *J. Appl. Phys.* **2016**, *119*, 014303.
- [57] J. R. Chen, P. M. Odenthal, A. G. Swartz, G. C. Floyd, H. Wen, K. Y. Luo, R. K. Kawakami, *Nano Lett.* **2013**, *13*, 3106.
- [58] A. Dankert, L. Langouche, M. V. Kamalakar, S. P. Dash, *ACS Nano* **2014**, *8*, 476.
- [59] M. Farmanbar, G. Brocks, *Adv. Electron. Mater.* **2016**, *2*, 1500405.
- [60] G. Pande, J. Y. Siao, W. L. Chen, C. J. Lee, R. Sankar, Y. M. Chang, C. D. Chen, W. H. Chang, F. C. Chou, M. T. Lin, *ACS Appl. Mater. Interfaces* **2020**, *12*, 18667.
- [61] H. Gao, J. Suh, M. C. Cao, A. Y. Joe, F. Mujid, K. H. Lee, S. Xie, P. Poddar, J. U. Lee, K. Kang, P. Kim, D. A. Muller, J. Park, *Nano Lett.* **2020**, *20*, 4095.
- [62] J. Jiang, L. Xu, C. Qiu, L. M. Peng, *Nature* **2023**, *616*, 470.
- [63] M. Liu, S. Shahi, S. Fathipour, W. Hwang, M. Remskar, A. Seabaugh, H. Li, in *2018 IEEE 13th Nanotechnology Materials and Devices Conf. (NMDC)*, IEEE, Portland, OR, USA October **2018**, pp. 1–4.
- [64] S. G. Louie, M. L. Cohen, *Phys. Rev. B* **1976**, *13*, 2461.
- [65] S. Lee, X. Wang, H. Shin, N. Ali, T. D. Ngo, E. Hwang, G. H. Kim, G. Y. Yeom, K. Watanabe, T. Taniguchi, W. J. Yoo, *ACS Appl. Electron. Mater.* **2024**, *6*, 4149.
- [66] I. A. Elisseyev, B. R. Borodin, D. R. Kazanov, A. V. Poshakinskiy, M. Remškar, S. I. Pavlov, L. V. Kotova, P. A. Alekseev, A. V. Platonov, V. Y. Davydov, T. V. Shubina, *Adv. Opt. Mater.* **2023**, *11*, 2202782.
- [67] P. Bolshakov, C. M. Smyth, A. Khosravi, P. Zhao, P. K. Hurley, C. L. Hinkle, R. M. Wallace, C. D. Young, *ACS Appl. Electron. Mater.* **2019**, *1*, 210.
- [68] R. Mahlouji, Y. Zhang, M. A. Verheijen, J. P. Hofmann, W. M. M. Kessels, A. A. Sagade, A. A. Bol, *ACS Appl. Electron. Mater.* **2021**, *3*, 3185.
- [69] B. J. Lee, B. J. Lee, J. Lee, J. W. Yang, K. H. Kwon, *Thin Solid Films* **2017**, *637*, 32.
- [70] J. J. Schwartz, H. J. Chuang, M. R. Rosenberger, S. V. Sivaram, K. M. McCreary, B. T. Jonker, A. Centrone, *ACS Appl. Mater. Interfaces* **2019**, *11*, 25578.
- [71] A. Jain, P. Bharadwaj, S. Heeg, M. Parzefall, T. Taniguchi, K. Watanabe, L. Novotny, *Nanotechnology* **2018**, *29*, 265203.
- [72] J. Pető, T. Ollár, P. Vancsó, Z. I. Popov, G. Z. Magda, G. Dobrik, C. Hwang, P. B. Sorokin, L. Tapasztó, *Nat. Chem.* **2018**, *10*, 1246.
- [73] S. Reinhardt, C. Butschkow, S. Geissler, A. Dirnacher, F. Olbrich, C. Lane, D. Schröer, A. K. Hüttel, *Comput. Phys. Commun.* **2019**, *234*, 216.